Continental Shelf Research 56 (2013) 13–25

Contents lists available at SciVerse ScienceDirect

Continental Shelf Research

journal homepage: www.elsevier.com/locate/csr

Research papers

Typhoons enhancing northward transport through the Taiwan Strait

Wen-Zhou Zhang [a,b,c,*], Hua-Sheng Hong [a,b,c], Xiao-Hai Yan [d]

[a] State Key Laboratory of Marine Environmental Science, Xiamen University, Xiamen, China
[b] Coastal and Ocean Management Institute, Xiamen University, Xiamen, China
[c] Fujian Provincial Key Laboratory for Coastal Ecology and Environmental Studies, Xiamen University, Xiamen, China
[d] Center for Remote Sensing, College of Earth, Ocean and Environment, University of Delaware, Newark, DE, USA

ARTICLE INFO

Article history:
Received 4 December 2012
Received in revised form
20 January 2013
Accepted 26 January 2013
Available online 13 February 2013

Keywords:
Volume transport
Dynamic mechanism
Typhoon
Taiwan Strait

ABSTRACT

Volume transport in the Taiwan Strait is usually northward for most of the year and varies seasonally because of the adjustment of the East Asian monsoon. Based on model simulations, the influence on this northward transport of every typhoon formed during the period 2005–2009 was examined. The results showed that there were four typhoons which enhanced northward transport during these five years. The current measurements, obtained from a buoy deployed in the Taiwan Strait, matched these events exactly. These typhoons had special moving tracks and life histories. They traveled westward in the area south of the strait or moved northward from the south to the north. Under the influence of such a typhoon, the prophase southward atmospheric forcing in the strait was weak and the anaphase northward atmospheric forcing (mainly along-strait wind stress) was strong, which is necessary and crucial in enhancing the northward transport. The ageostrophic process, another important driving factor in transport change, was generated mainly by local atmospheric forces inside the strait under the typhoon weather conditions and its effect on transport magnitude was comparable to that of direct atmospheric forcing. It first stored some energy from the atmospheric forcing to restrain the transport change, and then released the stored energy to prolong and even to intensify the enhanced northward transport.

1. Introduction

The Taiwan Strait, located at the western margin of the North Pacific, is about 350 km long, 180 km wide and 60 m deep on average (see Fig. 1). As the only channel joining the East China Sea (ECS) and the South China Sea (SCS), it plays an important role in water or mass exchange and heat transport between these two adjacent marginal seas.

Volume transport through the Taiwan Strait, which causes water to be exchanged between the SCS and the ECS, has prompted many investigations since the 1960s, but most of these focused on its seasonal or annual variation. The monthly mean transport is mainly northward in summer while it may be southward in winter (Wyrtki, 1961; Fu et al., 1991; Chai et al., 2001; Fang et al., 2003; Wu and Hsin, 2005; Jan et al., 2006). Although the reported estimates for its magnitude differ markedly, the crucial effects of the East Asia monsoon and the along-strait sea-level gradient on its seasonal variation are recognized (e.g. Wang et al., 2003; Guo et al., 2005; Lin et al., 2005). The transport correlates well with along-strait wind or wind stress, and two linear regression equations were provided by Wang et al. (2003) and Wu and Hsin (2005). In a diagnostic analysis based on the AVISO's satellite altimeter sea surface height anomaly data and the NCEP's monthly mean wind field data, Guo et al. (2005) argued that sea-level gradient is more important than local wind in controlling the variation.

Recently, the impacts of short-term extreme synoptic events on its short time-scale variation are reported in the literature (e.g. Ko et al., 2003 and Zhang et al., 2009). For such impacts, their dynamic mechanisms seem to be more complicated than the simple statistical relationships provided for seasonal variation. Ko et al. (2003) showed that northward transport in the Taiwan Strait is reversed by winter wind bursts via a combination of local wind and remote wind in the Yellow Sea and ECS. Barotropic coastally-trapped Kelvin waves, generated by northerly winds in the Yellow Sea and enhanced by alongshore northerly winds in the ECS, propagate southward into the strait and then induce transport reversals together with local winds. Typhoons, similar to hurricanes in the Atlantic, are severe weather systems frequently appearing in the western North Pacific. The Taiwan Strait is often affected by typhoons in the typhoon prevailing seasons. Strong northeasterly winds accompanying a typhoon cause northward Taiwan Strait outflow to decline and then modify the circulation to the north

* Corresponding author at: Xiamen University, Department of Physical Oceanography, College of Ocean and Earth Sciences, 422 Siming Nanlu, Xiamen, Fujian 361005, China. Tel.: +86 592 2184209; fax: +86 592 2095242.
E-mail address: zwenzhou@xmu.edu.cn (W.-Z. Zhang).

0278-4343/$ - see front matter © 2013 Elsevier Ltd. All rights reserved.
http://dx.doi.org/10.1016/j.csr.2013.01.019

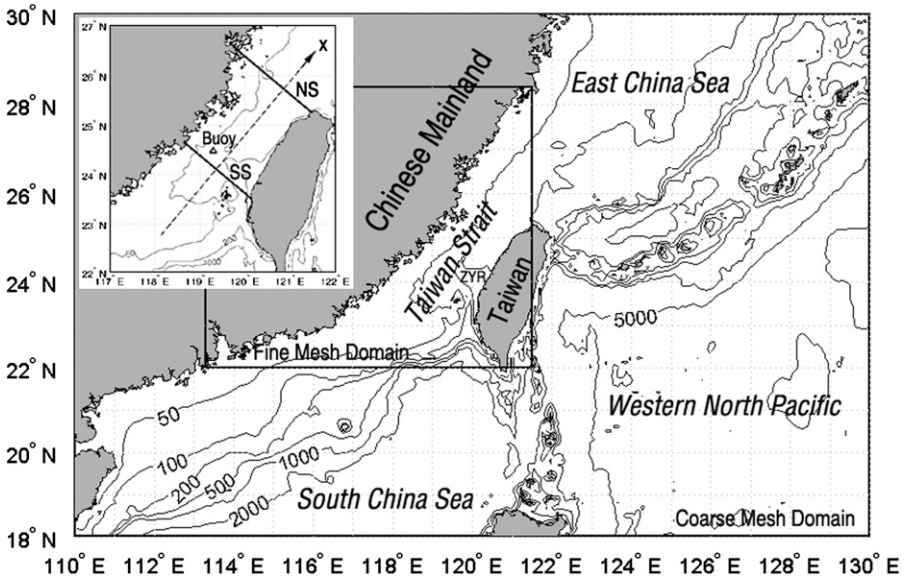

Fig. 1. The study area and model domain. Depth contours are in meters. The upper left map shows the locations of the sections (denoted by solid lines) and the buoy (denoted by a triangle). ZYR: the Zhang-Yun Ridge; NS: the northern section in the Taiwan Strait; SS: the southern section.

of Taiwan Island (Tsai et al., 2008). Furthermore, the northward current can be changed to southward, even in the bottom layer of this shallow strait, during typhoon periods (Chen et al., 2003; Zhang et al., 2009; Chang et al., 2010; Lin et al., 2010). Some typhoons induce strong southward transport events by typhoon-generated local wind stress and/or along-strait water level gradient, which temporarily reverse northward transport in the strait (Zhang et al., 2009; Chang et al., 2010).

As known from previous investigations, typhoons can temporarily reduce or even reverse the northward current and transport through the Taiwan Strait. However, this may not be true for all typhoons that affect this area. This paper will identify a few typhoons that intensified the northward current and enhanced northward transport. Such cases that have an inverse effect on transport could reveal to us some different and unknown stories. As counterexamples, they are also valuable and important for verifying the knowledge previously obtained from more usual cases. Therefore, investigating these infrequent cases may improve our understanding of the dynamic mechanisms by which typhoons influence transport through a shallow strait such as the Taiwan Strait, which is the aim of this study. For simplicity, here we uniformly call all strong tropical cyclones typhoons–but actually include tropical storms, severe tropical storms, typhoons, severe typhoons and super typhoons according to the grade of tropical cyclones published by China in 2006 (China Meteorological Administration, 2006).

This paper is organized as follows. Section 2 simply introduces the numerical model applied in this work and the data used to drive the model. Section 3 provides a method to classify typhoons according to their influence on the northward transport through the Taiwan Strait. We used this method to examine whether a typhoon enhanced northward transport. The calculated results and dynamic analyses for the typhoons which enhanced the northward transport are presented in Section 4. In the last section, the results are discussed and conclusions drawn.

2. Numerical model and driving forces

Since the Taiwan Strait is a shallow channel with an average depth of about 60 m and volume transport is a depth-integrated result, the baroclinic effect and vertical structure of currents are not taken into account. Chuang (1985) demonstrated that the pressure gradient generated by the baroclinic effect of current can be easily overcome by atmospheric forcing due to the broadness and shallowness of the strait. Periodic tidal movement is not considered because it has little influence on net transport through the strait. A two-dimensional barotropic numerical model, developed by Zhang et al. (2007) and Zhang et al. (2009), was adopted in this study. This model is based on shallow water equations in spherical coordinates, including depth-averaged continuity and momentum equations. The shallow water model can describe important aspects of oceanic motion, except for the phenomena associated with stratification and baroclinicity. More importantly, avoiding the complexities of the thermodynamics of a fluid, it allows the essential dynamic characteristics to be easily identified (Pedlosky, 1987). Additionally, the depth-averaged current defined in the shallow water model is consistent in form with unit-width volume transport divided by total water depth. We could calculate unit-width transport directly from depth times depth-averaged current without additional error due to the vertical discretization of current in a three-dimensional model.

The model domain is shown in Fig. 1, comprising two different-resolution grid meshes. The coarse mesh covers a large area (110–130°E, 18–30°N) with a resolution of 1/10° and the fine one has a small area (113.3–121.5°E, 22.0–28.4°N) with a resolution of 1/30°. The former entirely mantles the latter. These two meshes were nested using a two-way nesting technique (Zhang et al., 2007). The current and water level simulated by the coarse mesh model were first provided for the radiation boundary conditions of the fine mesh following Flather (1976) and then the water-level results calculated for the fine mesh were fed back to the coarse mesh, namely the averaged water elevation of all fine grid cells within a coarse grid cell replaced the previously simulated value of the coarse grid cell. This process was conducted once in every time-step.

The data used to drive the model included surface wind (10 m above the sea surface), air pressure at mean sea level, and ocean current at the open boundaries of the coarse mesh. The wind fields were derived by merging remotely sensed observations from satellites (including the QuikSCAT and the Defense Meteorological Satellites Program satellites F13–F15) and operational ECMWF wind analyses (referred to as the blended wind hereafter), which was performed by the CERSAT at IFREMER, France. They have a

spatial resolution of $0.25^\circ \times 0.25^\circ$ and a temporal resolution of 6 h, covering a time period 1 April 2004 to 22 November 2009 prior to the failure of the QuikSCAT satellite. This blended wind data set compared well with remotely sensed wind estimates and buoy observations, including buoy observations in the Taiwan Strait (Zhang et al., 2009). The air pressure fields were taken from the global mean sea level pressure data set of the ECMWF Interim Reanalysis with a spatial resolution of $0.75^\circ \times 0.75^\circ$ and a temporal spacing of 6 h. The currents at the open boundaries were obtained from the five daily ocean reanalysis data sets of the NCEP Global Ocean Data Assimilation System which has a resolution of 0.33° latitude and 1.00° longitude and 40 levels in the vertical direction. The impact of ocean circulations and meteorological driving forces outside the model domain on the currents inside the model domain was taken into account by momentum input to the open boundary conditions. All these data sets were spatially interpolated to the model grids via the two-dimensional bicubic interpolation method and temporally to every time step via linear interpolation.

The model was firstly spun up from rest for six months to reach a quasi-equilibrium state using the monthly average atmospheric and current data of April, 2004. Then it continued to be forced with the above-described data sets from 1 May 2004 to 22 November 2009. The simulated results of the period 1 January 2005 to 22 November 2009 were used for this study.

This model was validated by Zhang et al. (2007,2009) who showed that it works well in the Taiwan Strait. We do not repeat its validation here for simplicity, but more details concerning the model are given in the references cited above.

3. Classifying method

Two time series of total transport through the southern and the northern sections across the Taiwan Strait (denoted by SS and NS in Fig. 1) were calculated from the numerical model results described previously. Both series had the same mean value of 0.77 Sv and standard deviation of 1.30 Sv, and the correlation coefficient between them was 0.9996 at the 99% significance level. The mean absolute value of difference between them was only 0.03 Sv and the corresponding standard deviation was 0.04 Sv. This demonstrated that they varied synchronously and had little difference in magnitude, indicating that transport is through the entire strait and not sensitive to section location. Thus, only the transport series through the southern section, which is near to the buoy deployed in the strait (Fig. 1), will be used hereafter.

Typhoons, based on their effects on the northward transport through the Taiwan Strait, could be divided into four types according to the following criteria:

(1) Positive: $\frac{Q_N - Q_S}{t} > \alpha Q_{std}, \quad t > 0;$
(2) Negative: $\frac{Q_S - Q_N}{t} > \alpha Q_{std}, \quad t > 0;$
(3) Balanced: $\frac{|Q_N - Q_S|}{t} \le \alpha Q_{std}, \quad t > 0;$
(4) No influence: $Q_N = 0, \quad Q_S = 0,$ or $t = 0.$

where Q_{std} is the standard deviation of the transport time series deviating from 30-day running averages, Q_S the cumulative negative effect (below one standard deviation from the 30-day running average of the transport) of a typhoon on the northward transport, and Q_N the cumulative positive contribution (above one standard deviation from the running average); t is the time period from the beginning to the end of a typhoon inducing abnormal transport (surpassing one standard deviation from the running average); α is an empirical dimensionless constant which was set to be 0.05. Mathematically, Q_S is the area between the transport series curve and the curve denoting one standard deviation below the running average; it could be calculated using the following formula:

$$Q_S = \begin{cases} \int_t [(Q_m - Q_{std}) - Q]dt, & Q < Q_m - Q_{std} \\ 0, & Q \ge Q_m - Q_{std} \end{cases}, \quad (1)$$

where Q is the transport through the southern section and Q_m is the 30-day running average. Similarly, Q_N could be calculated using the following formula:

$$Q_N = \begin{cases} \int_t [Q - (Q_m + Q_{std})]dt, & Q > Q_m + Q_{std} \\ 0, & Q \le Q_m + Q_{std} \end{cases} \quad (2)$$

The classification of typhoons could quickly be carried out using a computer program and following the above criteria. However, we should carefully check the results of some special cases. When two or more typhoons appeared almost in the same period, we should artificially judge which of them really changed the transport violently and then determine their types separately. In later autumn and winter, an abnormal transport event might have been caused by wind burst, as Ko et al. (2003) indicated, rather than a typhoon which appeared at the same time. For these two cases, it was not difficult to deduce whether a typhoon significantly influenced the transport by examining the distance between its moving track and the Taiwan Strait and/or by analyzing QuikSCAT remote sensing wind fields during its lifetime.

Typhoons belonging to type 1 had a positive net effect on northward transport or enhanced northward transport through the Taiwan Strait overall while type 2 typhoons had a negative net effect. Actually the latter often induced a strong southward transport event as Zhang et al. (2009) showed. For type 3 typhoon, its positive contribution to northward transport was almost balanced by its negative effect, thus its net effect nearly equaled zero. The type 4 typhoon was usually far away from the strait during its lifetime or was too weak to distinctly influence transport, and consequently had neither positive nor negative effects. Apparently, it was different from the type 3 typhoon, although both of them actually had no net effect on transport.

4. Results and analyses

4.1. Results

Following the method presented in the previous section, we classified 116 typhoons which appeared in the western North Pacific (including its marginal seas) during the period 1 January 2005 to 22 November 2009. The last typhoon in 2009, formed after 22 November, was not included, but it could be definitely classified into type 4 since its track was far away from the Taiwan Strait throughout its lifetime.

Among these 117 typhoons, 74 (about 63%) had no perceptible influence on transport through the Taiwan Strait (see Table 1, type 4). As anticipated, they always moved around in the sea area

Table 1
Classification of typhoons according to their effects on northward transport through the Taiwan Strait.

Year	Typhoons	Positive (type 1)	Negative (type 2)	Balanced (type 3)	No influence (type 4)
2005	23	0	8	1	14
2006	24	0	8	0	16
2007	25	1	7	1	16
2008	22	2	7	0	13
2009	23	1	7	0	15
Total	117	4 (3.4%)	37 (31.6%)	2 (1.7%)	74 (63.2%)

far away from the Taiwan Strait or became very weak before they came near to the strait. As seen from Table 1, only two typhoons (nearly 2%) belonged to type 3, i.e., they had no overwhelmingly positive or negative effect on northward transport but, although they made little contribution to the mean transport during their lifetimes, they often forced instantaneous transport to fluctuate drastically. There were 37 typhoons (nearly 32%) which exerted a prominent, negative influence on northward transport (type 2 in Table 1). They usually induced strong southward transport events in the strait as Zhang et al. (2009) noted. Only four typhoons (about 3%) had an evident, positive effect, namely enhancing northward transport (type 1, see Fig. 2). Since Zhang et al. (2009) have demonstrated the dynamic mechanisms of how typhoons reduce or even reverse northward transport, these four unusual typhoons will be emphasized in the following part of this paper.

The tracks of the four typhoons mentioned above are shown in Fig. 3. Two of them traveled from east to west in the sea area to the south of the strait and the other two migrated northward and passed by the strait. All of them appeared in summer (June to August) when a weak southwest monsoon wind usually dominates in this area and transport in the Taiwan Strait is principally northward. Three typhoons, including Pabuk (2007), Kalmaegi (2008) and Linfa (2009), were near to the strait with maximum sustained winds below 33 m s^{-1} while the other typhoon, Nuri (2008), was far from the strait with a maximum sustained wind of 40 m s^{-1}.

4.2. Typhoons enhancing northward transport through the Taiwan Strait

4.2.1. Equation controlling transport through the Taiwan Strait

Based on depth-averaged momentum and continuity equations, Zhang et al. (2009) obtained a transport equation for the Taiwan Strait, assuming that both banks of the strait are in parallel with x coordinate in a Cartesian coordinate system and no water is allowed to flow through coastal boundaries. Here the x coordinate is to the northeast along the midline of the strait (shown in Fig. 1) and the y coordinate is to the northwest across the strait (not shown). Then the transport equation could be written as follows:

$$\underset{\text{CRT}}{\frac{\partial Q}{\partial t}} = \underset{\text{MGT}}{-\int_{-b/2}^{b/2}\frac{\partial HU^2}{\partial x}dy} \underset{\text{WGT}}{-\int_{-b/2}^{b/2}(C^2\frac{\partial \zeta}{\partial x})dy} \underset{\text{CFT}}{+\int_{-b/2}^{b/2}fHVdy} \underset{\text{BFT}}{-\int_{-b/2}^{b/2}\frac{F_b}{\rho}dy} \underset{\text{WST}}{+\int_{-b/2}^{b/2}\frac{F_s}{\rho}dy} \underset{\text{AGT}}{-\int_{-b/2}^{b/2}\frac{H}{\rho}\frac{\partial p_a}{\partial x}dy}, \quad (3)$$

$$Q = \int_{-b/2}^{b/2} HUdy, \quad (4)$$

where U is the depth-averaged along-strait current component, V the depth-averaged cross-strait current component and t the time; F_b is the bottom stress, F_s the wind stress and p_a the air pressure; ρ is the constant density of sea water; b and H denote the width and the depth of the strait, respectively, and $C=\sqrt{gH}$ in which g is the gravitational acceleration. The first term on the right hand side of Eq. (3) (referred to as MGT) presents the along-strait momentum gradient in the strait, which originates from the

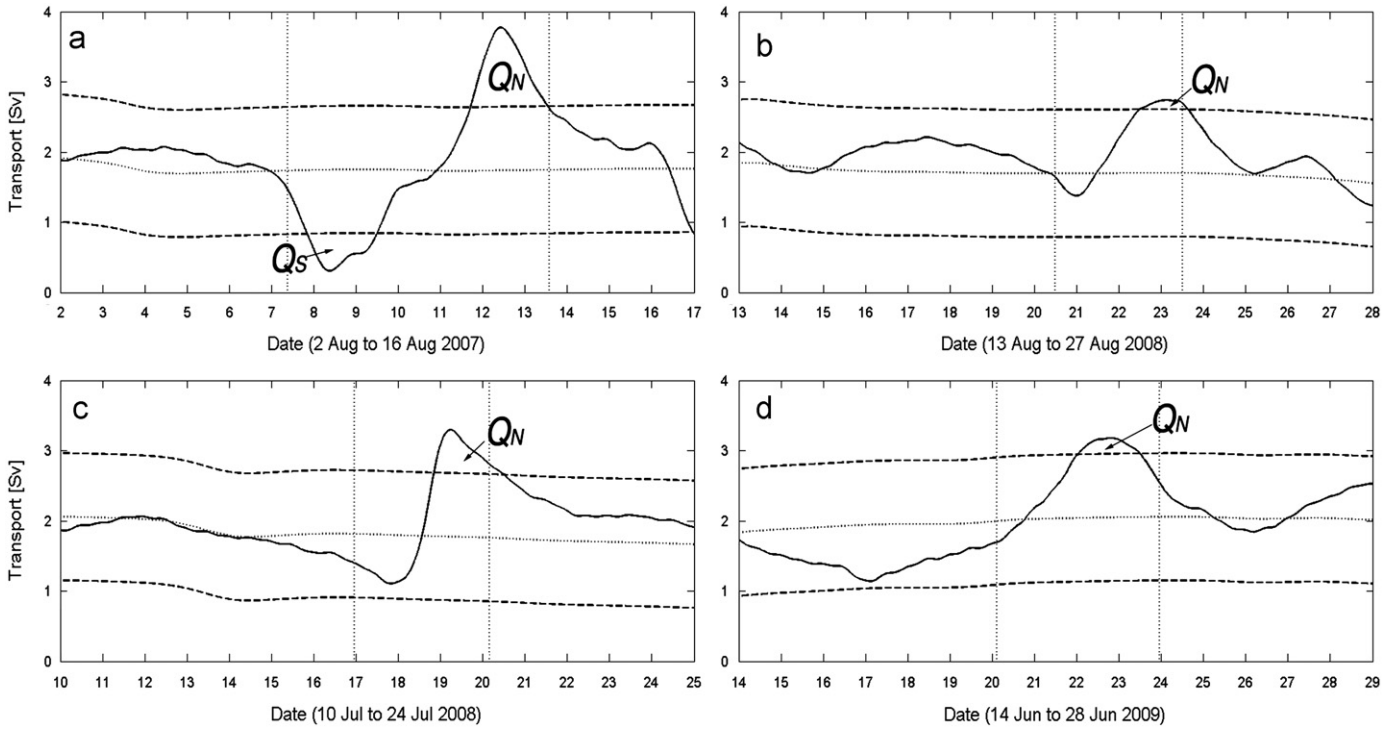

Fig. 2. Time series of transport through the Taiwan Strait during Typhoons (a) Pabuk (2007), (b) Nuri (2008), (c) Kalmaegi (2008), and (d) Linfa (2009). The solid lines denote the transport, dotted lines the 30-day running averages, and dashed lines one standard deviation values from 30-day running averages. The time period between two vertical dotted lines in every panel is the period of influence of the typhoon on the strait. Q_N and Q_S are the areas enclosed by the solid line and the dashed lines, indicating cumulative positive and negative effects of a typhoon on northward transport, respectively.

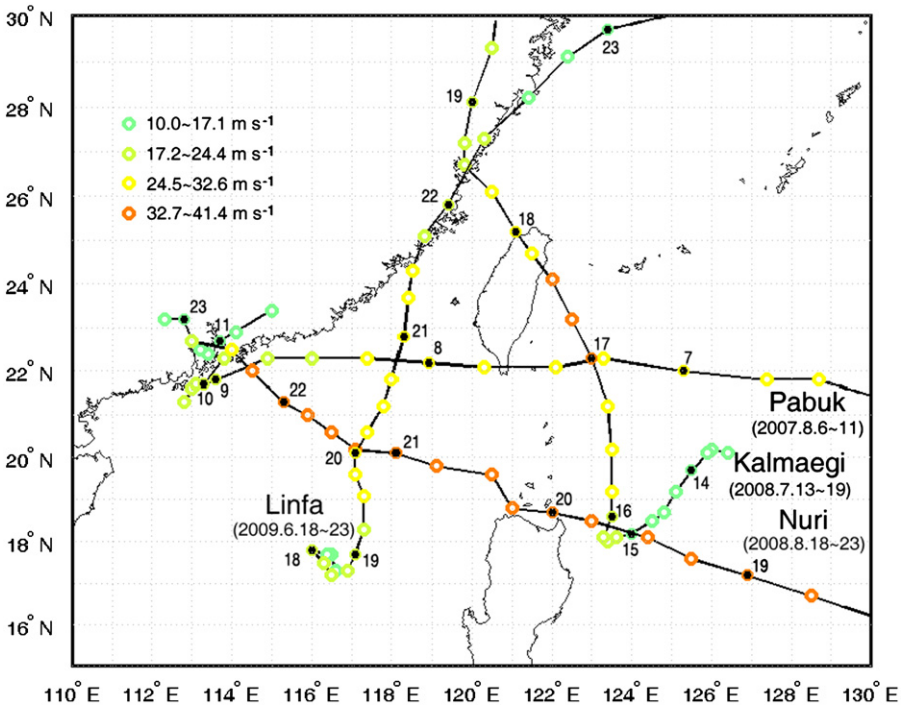

Fig. 3. The best tracks of the typhoons which enhanced northward transport through the Taiwan Strait during the period 2005–2009. Black dots denote typhoon positions at 0800 local standard time (LST) on the dates labeled by corresponding numbers and circles denote typhoon positions at 0200, 1400, or 2000 LST, together with their different strengths color coded.

nonlinear along-strait convective term; the second term (referred to as WGT) is related to the water level gradient in the along-strait direction; the third (referred to as CFT) is associated with the Coriolis force; the fourth is the bottom friction term (BFT) which is dependent on flow velocity according to a quadratic law; and the last two terms are atmospheric forcing terms—wind stress term (WST) and air-pressure gradient term (AGT). This equation describes the essential dynamic relationship between the transport variation and potential driving factors whereby the change rate of transport (CRT) is determined by the combination of all above terms (CAT).

Every term in Eq. (3) could be calculated in the numerical model described previously after the equation was approximately rewritten in its discrete difference form. Note that before doing this, all variables in these terms should be equivalently expressed by variables in the spherical coordinate system employed by the model. Figs. 4–7 show that the CRT series is in excellent agreement with the CAT although they are independently calculated from data, indicating the validity of this equation in the Taiwan Strait. Based on the results of these terms, in the following subsections we will analyze the possible dynamic mechanisms by which the above-mentioned typhoons enhanced northward transport through the Taiwan Strait.

4.2.2. Typhoon Pabuk (2007)

Typhoon Pabuk (2007) was formed in the western North Pacific on 5 August 2007 and moved westward almost along 22° latitude, quickly passing by the southern end of the Taiwan Strait. It was not a strong tropical cyclone with a maximum wind speed of 30 m s^{-1}. When it came near to the coastline of South China after midday on 8 August, it moved slowly for over three days in the coastal area, with its maximum wind speed decreasing.

As seen from Fig. 4a, the negative WST decreased slowly when Pabuk came near to the strait before 8 August (see Fig. 3), indicating that along-strait southward wind stress gradually became strong due to the approach of Pabuk. After Pabuk entered the strait in the early morning of 8 August, the negative WST increased to zero and then became positive. Accompanying this process, northward (positive) transport through the Taiwan Strait first decreased below one standard deviation from the averaged value and reached its minimum in the morning of 8 August, then relaxedly increased to normal after the southward wind stress disappeared (Figs. 2a and 4a). When Pabuk came near to the coast of South China on 10 August, the northward wind in its eastern portion began to affect the Taiwan Strait and the positive WST increased. Meanwhile, the northward transport strengthened synchronously. The WST and transport reached their maxima almost at the same time and subsequently both decreased when Pabuk died away. Thus, along-strait wind stress must have played an important role in the transport variation.

The air-pressure gradient force is associated with the location of the typhoon center, since a typhoon is not only a cyclonically rotating wind system but also a low-pressure system. Since Pabuk moved in the area south of the Taiwan Strait (Fig. 3), the along-strait component of air-pressure gradient force was mainly southward and thus against northward transport, showing up as a negative AGT in Fig. 4a. It is clear that the AGT was much smaller than the WST.

It can be seen from Fig. 4a that the WGT was negative and the CFT was positive. Although the absolute values of both terms were much larger than those of the WST, they mostly canceled each other because of the geostrophic balance between the water level gradient force and the Coriolis force in the low frequency band. Actually, the ageostrophic effect (WGT plus CFT) influenced transport through the Taiwan Strait according to Eq. (3). Fig. 4b shows that the ageostrophic effect was comparable in magnitude to the WST. Its positive value demonstrated that the CFT overwhelmed the WGT during the period 2–16 August 2007. This ageostrophic effect obviously tended to restrain the reduction of northward transport when the southward wind strengthened with the approach of Pabuk, and made some contribution to northward transport during the period 8–12 August. Additionally,

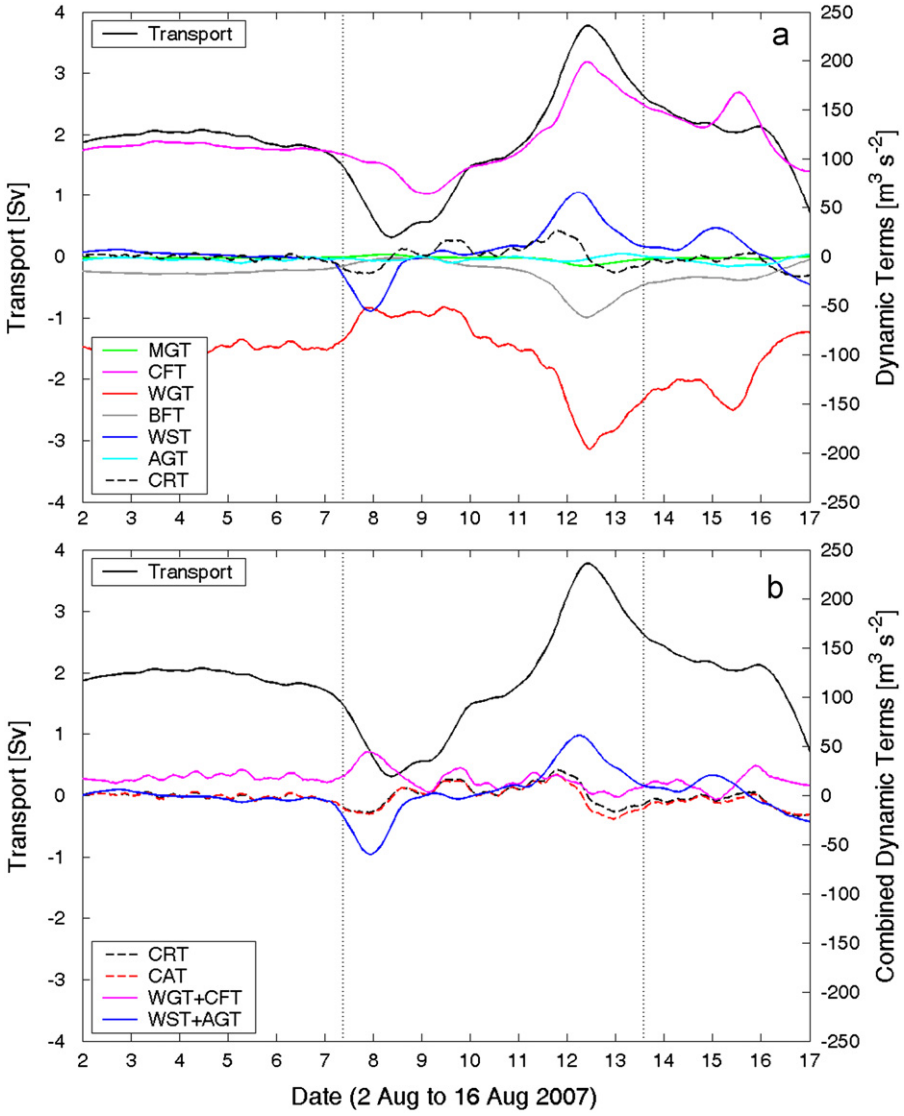

Fig. 4. Time series of transport through the Taiwan Strait and its change rate with (a) relevant dynamic terms and (b) their combinations during Typhoon Pabuk (2007). The positive is northward along the strait and the negative is southward. MGT: momentum gradient term; CFT: Coriolis force term; WGT: water-level gradient term; BFT: bottom friction term; WST: wind stress term; AGT: air-pressure gradient term; CAT: the combination of all above terms; CRT: change rate of transport. The time period between two vertical dotted lines is the period of influence of the typhoon on the strait.

its effect was responsible for the apparent fluctuations of the CRT during this period (Fig. 4b). The BFT had a negative effect on transport and its magnitude changed with the strength of the transport (Fig. 4a). The small value of the MGT indicated that this term had little effect on transport during the lifetime of Pabuk.

The anaphase positive effect of the CAT lasted for a longer period (about four days) than the prophase negative effect during the period of influence of Pabuk. Also the former was larger, mainly because the northward along-strait wind stress was stronger in the late stage of Pabuk (after 10 August) than the southward along-strait wind stress in the early stage (before 9 August) as indicated by the WST in Fig. 4a. This resulted in the northward transport being enhanced as a whole, together with the ageostrophic effect.

4.2.3. Typhoon Nuri (2008)

Typhoon Nuri (2008) traveled west-northwest through the southern part of the Luzon Strait and across the northeast SCS with a radius of 350 km on the Beaufort wind scale No. 7, and finally landed on the coast of South China in the afternoon of 22 August 2008 (Fig. 3). It was somewhat stronger, with a maximum wind of 40 m s^{-1}, than Typhoon Pabuk (2007), but its track was some distance away from the Taiwan Strait.

Fig. 5 shows that northward transport through the Taiwan Strait decreased a little before 21 August 2008 when Nuri came near to the strait, and then increased gradually to exceed one standard deviation from the running-averaged transport (Fig. 2b). The enhanced northward transport returned to the average value after 24 August, when Nuri moved far away from the strait. The WST showed a synchronous, similar process: first decreasing a little, then increasing slowly and finally degrading. This corresponded to a weak southward wind with the approach of Nuri and a northward wind with its departure. The AGT was always negative during Nuri for the same reason as during Typhoon Pabuk. The combination of the WST and the AGT, indicating total atmospheric forcing, had a similar variation to the WST although the negative AGT offset partly the positive WST (Fig. 5).

The CFT and the WGT were obviously disturbed by Typhoon Nuri (Fig. 5a). The CFT decreased with a southward wind (negative WST) and increased with a northward wind (positive WST). Meanwhile, the negative WGT first rose and then dropped. Although the magnitudes of both the CFT and WGT were much

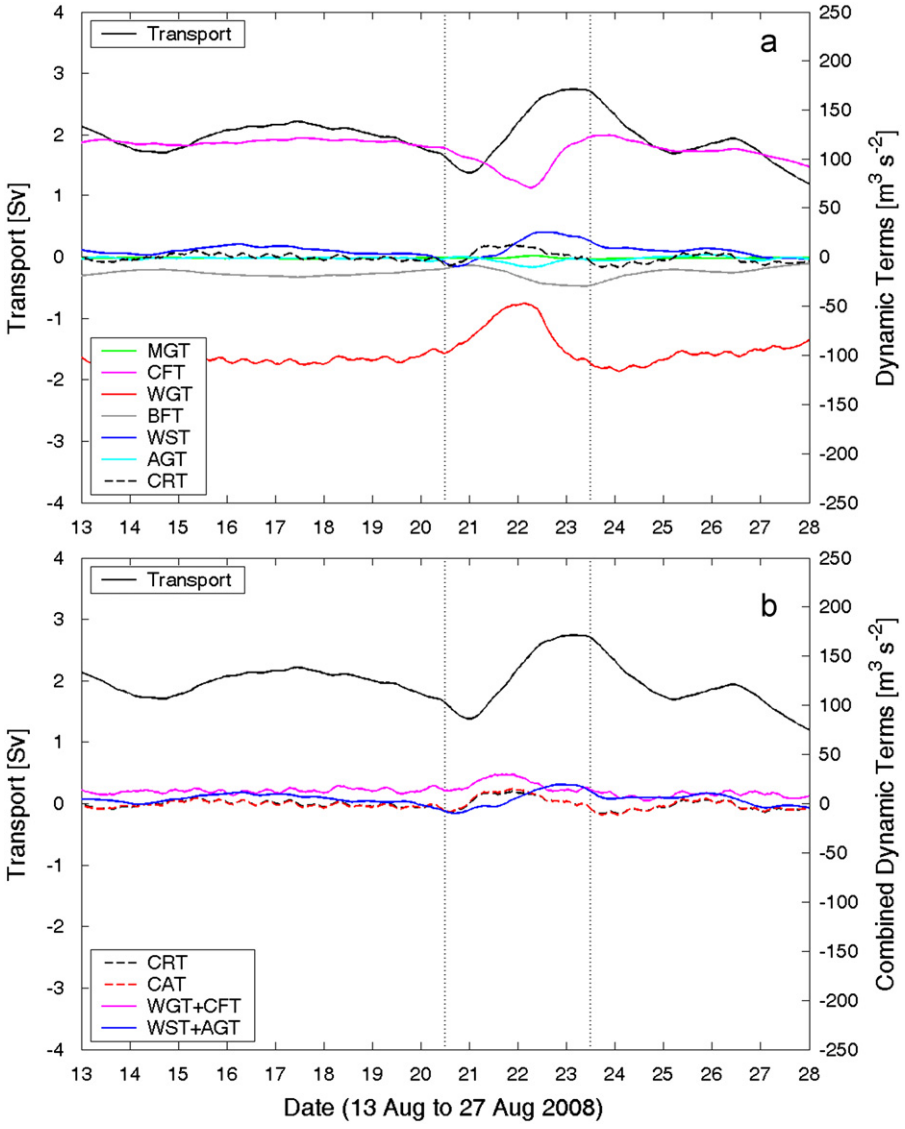

Fig. 5. As in Fig. 4, but for Typhoon Nuri (2008).

larger than that of the WST, their combination (ageostrophic effect) was comparable to the WST plus the AGT (Fig. 5b). The BFT was negative and changed inversely with the northward transport. The MGT was negligible compared with other terms.

The southward along-strait wind stress caused a negative CAT and weakened the northward transport at the early stage of Nuri. After that, the CAT changed to be positive with the recession of the southward wind stress and the augmentation of the northward ageostrophic effect. Northward transport, therefore, recovered quickly and further strengthened to surpass one standard deviation above the average when the wind stress turned north at the late stage of Nuri. The ageostrophic process resisted the reduction of the northward transport and contributed to its recovery. Nuri totally enhanced northward transport since an abnormal northward transport event was induced, as indicated by detided current measurements obtained from the previously mentioned buoy (see Fig. 8a).

4.2.4. Typhoon Kalmaegi (2008)

The track of Typhoon Kalmaegi (2008) which basically moved northward (see Fig. 3) is totally different from those of the westward-moving typhoons mentioned previously. Kalmaegi first moved southwestward with its intensity increasing after it was formed in the sea area east of the Luzon Strait on 13 July 2008. Then it turned around and moved north-northwestward after 16 July, approaching the northern part of Taiwan Island. Its intensity reached a maximum with a wind speed of 33 m s^{-1} before it landed on the island at the end of 17 July. After skipping over the northern Taiwan Island and moving across the northern end of the Taiwan Strait, it landed again on the coast of the Chinese mainland late on 18 July. Finally, it traveled northward and died out in the north.

Fig. 6a shows that northward transport was reduced slightly before Kalmaegi landed on the northern coast of Taiwan Island. A small negative WST indicated weak southward wind stress along the Taiwan Strait. On the contrary, the AGT became positive and increased with the northward movement of Kalmaegi. Both the positive CFT and the negative WGT shrank a little during this period, but their combination had no obvious trend of change (Fig. 6b). Thus the weak southward wind stress was the only factor responsible for the slight reduction of the northward transport before Kalmaegi landed on the island.

After this, the WST changed to be positive and increased quickly, indicating that the wind direction changed to be northward and the wind speed strengthened rapidly. The AGT reached its maximum on 18 July when the center of Kalmaegi moved to

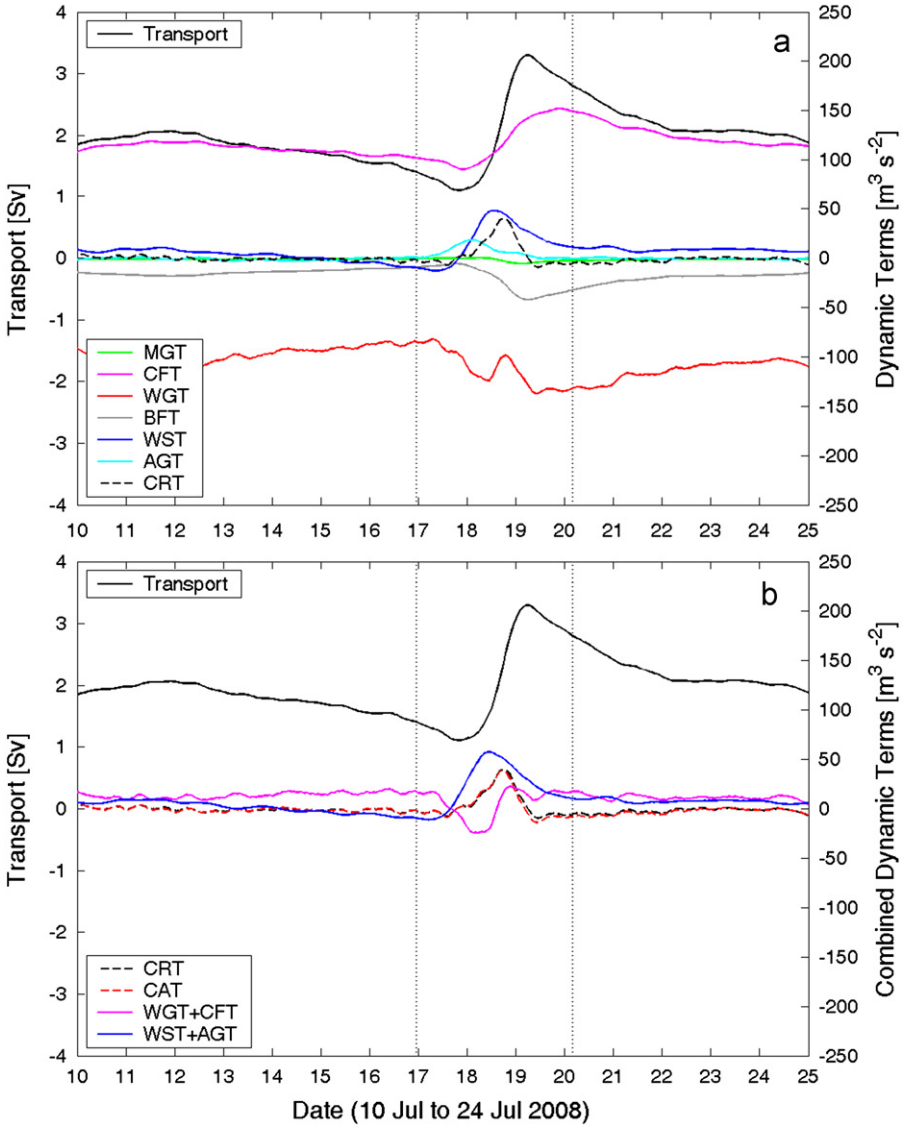

Fig. 6. As in Fig. 4, but for Typhoon Kalmaegi (2008).

the northern end of the Taiwan Strait. Thus, the air pressure gradient force was northward due to low pressure in Kalmaegi's central area. Obviously the AGT was smaller than the half of the WST (see Fig. 6a and Table 2). The positive WST and AGT both forced northward transport to strengthen. The negative WGT was first stronger and then weaker than the positive CFT, resulting in a violent oscillation of the ageostrophic effect (WGT plus CFT). Accordingly, the ageostrophic effect first restrained northward transport but subsequently enhanced it (Fig. 6b). The BFT strengthened due to the accelerating northward current, but its negative effect did not prevent northward transport from increasing (Fig. 6a). Thus, northward transport was enhanced to outstrip one standard deviation above the running average (see Fig. 2c) by both the atmospheric forcing and the ageostrophic process. The transport regressed to its normal range after Kalmaegi moved far away from the strait. This process was also recorded by current measurements of the buoy in the strait (Fig. 8b).

4.2.5. Typhoon Linfa (2009)

Typhoon Linfa (2009) had a unique track (see Fig. 3). It formed in the SCS on 18 June 2009, moved northward almost along a straight line after 19 June and disappeared in the north after 24 June. It is interesting that the center of the typhoon almost traveled along the west bank of the Taiwan Strait after it entered the strait. Thus, when the typhoon passed by, the strait was covered in its eastern part where the northward wind prevailed. Linfa was a weak tropical cyclone with a maximum wind speed of 30 m s^{-1} and a maximum radius of 260 km on the Beaufort wind scale No. 7.

Before Linfa entered the Taiwan Strait, the west-northwestward wind in the northern part of the typhoon dominated the strait, so the along-strait component of the wind was very weak. This resulted in a small, positive WST as shown in Fig. 7a. The negative AGT dropped further with the approach of Linfa, indicating a strengthening southward air-pressure gradient forcing. The negative value of the WST plus the AGT implied that the total atmospheric forcing was southward (Fig. 7b), contrary to the northward transport, at this stage of the typhoon. The ageostrophic effect of the WGT and CFT was positive and expanded, mainly because the negative WGT weakened during this period. The positive ageostrophic effect exceeded the negative effect of atmospheric forcing and the BFT, and caused the northward transport to strengthen when Linfa came near to the strait.

After Linfa entered the strait on 21 June, the wind in the Taiwan Strait changed to be northeastward and thus the WST

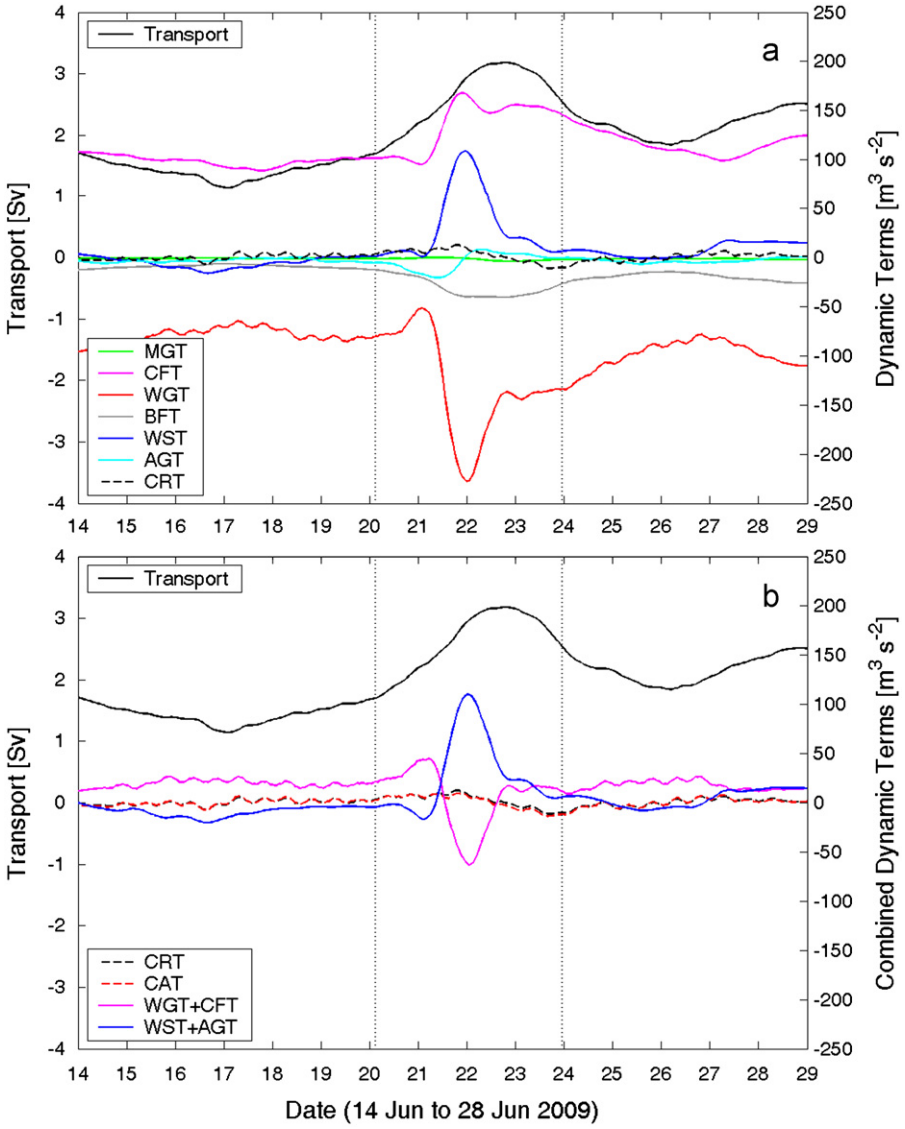

Fig. 7. As in Fig. 4, but for Typhoon Linfa (2009).

quickly increased. The positive WST reached its maximum when Linfa passed by the southern section at the beginning of 22 June and then decreased with the departure of Linfa (Figs. 3 and 7a). Meanwhile, the negative AGT increased and became positive when Linfa was in the northern part of the strait. The combination of the WST and the AGT varied mainly with the WST since the AGT was much smaller than the WST. During this process, the positive CFT increased swiftly, indicating a strengthening northwestward current component; The negative WGT decreased rapidly because the strong onshore wind in the northern portion of the typhoon generated a considerable storm surge which enhanced the northward water level gradient. The combination of WGT plus CFT, the ageostrophic effect, changed to negative and became prominent due to the overwhelming WGT. At this stage of the typhoon, northward transport was abnormally enhanced (Fig. 2d) by the WST associated with the northeastward wind despite the negative effect of both the ageostrophic process and the BFT. The depth-averaged current measurements at the buoy in the strait also showed a strengthening northward current event (Fig. 8c), which coincided with the enhanced northward transport. All these dramatic variations decayed with the departure of Linfa.

5. Discussion and conclusion

Four of the 117 typhoons formed during the period 2005–2009 enhanced northward transport through the Taiwan Strait. These unexpected events represented a very small proportion of all typhoons, but they revealed some particular dynamic processes which influenced transport.

During these events, local atmospheric forcing in the Taiwan Strait, especially along-strait wind stress (indicated by the WST), was a principal driving factor. The variation of along-strait wind depends on the moving track of a typhoon relative to the strait. The four typhoons had distinctive paths and a moderate, mildly varying strength. They moved westward in the sea area south of the strait or traveled from the south to the north past the strait. When such a typhoon came near the strait, the wind in its northern part had a large angle to the axis of the strait (such as Pabuk, Nuri, and Linfa) and/or was blocked by the high mountains (above 3000 m) on Taiwan Island (such as Pabuk and Kalmaegi). Then the typhoon continued to move westward away from the strait or travel northward. At this time, the wind in its southeastern (e.g. Kalmaegi) or eastern (e.g. Linfa) part had a small angle to the axis and blew into the strait without any blocking.

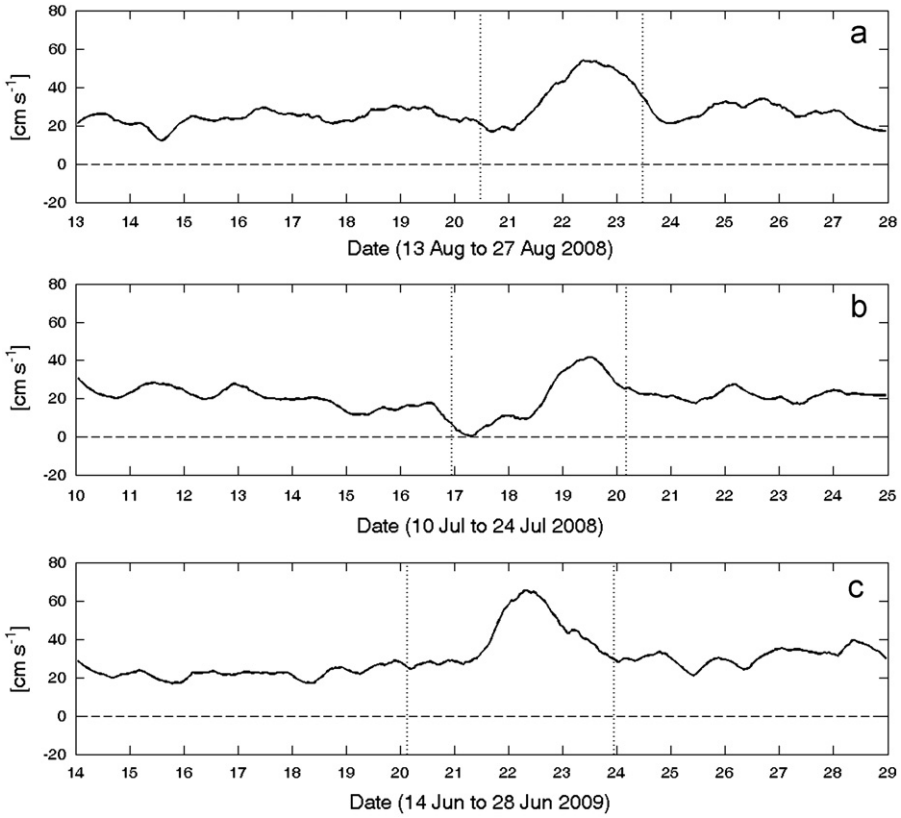

Fig. 8. Time series of detided, depth-averaged along-strait currents (cm s^{-1}) obtained from the buoy in the Taiwan Strait during Typhoons (a) Nuri (2008), (b) Kalmaegi (2008), and (c) Linfa (2009). The time period between two vertical dotted lines in every panel is the period of influence of the typhoon on the strait.

Consequently, the southward along-strait wind was weak in the early stage of the typhoon while the northward wind was strong in the late stage. This could, for the most part, have explained why northward transport was first reduced slightly and subsequently strengthened markedly during these events. The contribution of the air-pressure gradient force (indicated by the AGT) to the change of transport was much smaller than that of the along-strait wind stress, as deduced from the comparisons between maximum WST and AGT in Table 2.

The dynamic mechanism by which along-strait wind influences transport through the Taiwan Strait is generally explained by the along-strait wind changing sea surface slope across the strait via Ekman transport, and then additional through-strait transport is generated by the geostrophic balance between cross-strait Coriolis acceleration and water level gradient (Wyrtki, 1961; Ko et al., 2003). We checked the applicability of this concept under the severe influence of typhoons. Fig. 9 shows the comparison between the transport simulated directly by the model and that calculated from the water level gradient across the strait based on the geostrophic balance (referred to as geostrophic transport). Note that the water level gradient was adjusted for the inverted barometer effect. The geostrophic transport was basically in agreement with the simulated transport although it was slightly overestimated at most times due to ignoring other factors such as bottom friction in the momentum balance. However, it obviously deviated from the simulated transport during the periods of influence of Typhoons Pabuk, Kalmaegi and Linfa. Therefore, geostrophic transport could not satisfactorily describe the variation of realistic transport through the strait under the severe influence of typhoons. In other words, the above mechanism was not adequate to explain the influence of typhoons on transport and an additional process must have existed.

Known from the analyses of all terms in the simulated integral momentum equation, the ageostrophic process was also significant

Table 2
Maximum wind stress term (WST) and maximum air–pressure gradient term (AGT) during 15-day periods around Typhoons Pabuk (2007), Nuri (2008), Kalmaegi (2008), and Linfa (2009).

	Pabuk	Nuri	Kalmaegi	Linfa
Maximum WST ($m^3\ s^{-2}$)	65.47	24.94	47.92	108.70
Maximum AGT ($m^3\ s^{-2}$)	2.03	0.25	16.68	7.68

in the dynamic balance during the typhoon events described previously. Both the along-strait water level gradient force term and the Coriolis force term were very large, even larger than the wind stress term, but their effects were mostly canceled by geostrophic balance. It was their residual (WGT plus CFT, ageostrophic effect) that affected the variations of transport although along-strait water level gradient was a direct driving factor (Zhang et al., 2009). The ageostrophic effect was very small under non-typhoon weather conditions (Figs. 4–7b) suggesting a rough balance between the Coriolis and sea level gradient forces in the along-strait direction, and this was consistent with previous observations on the shelf (Pettigrew, 1981; Marmorino, 1983). However, it became unusually prominent under the severe influence of typhoons, comparable to the atmospheric forcing effect (WST plus AGT). The ageostrophic process, such as storm surges, could be generated by local atmospheric forces. As a response of the sea to strong atmospheric forcing, the ageostrophic process first stored some energy from atmospheric forcing; then it released the stored energy to maintain and even to intensify the enhanced northward transport through the strait, which can be seen in Figs. 4–7b.

The ageostrophic process could also be produced partly by the remote forcing effect of atmospheric forces, long waves and ocean circulation outside the Taiwan Strait. In order to examine this, we

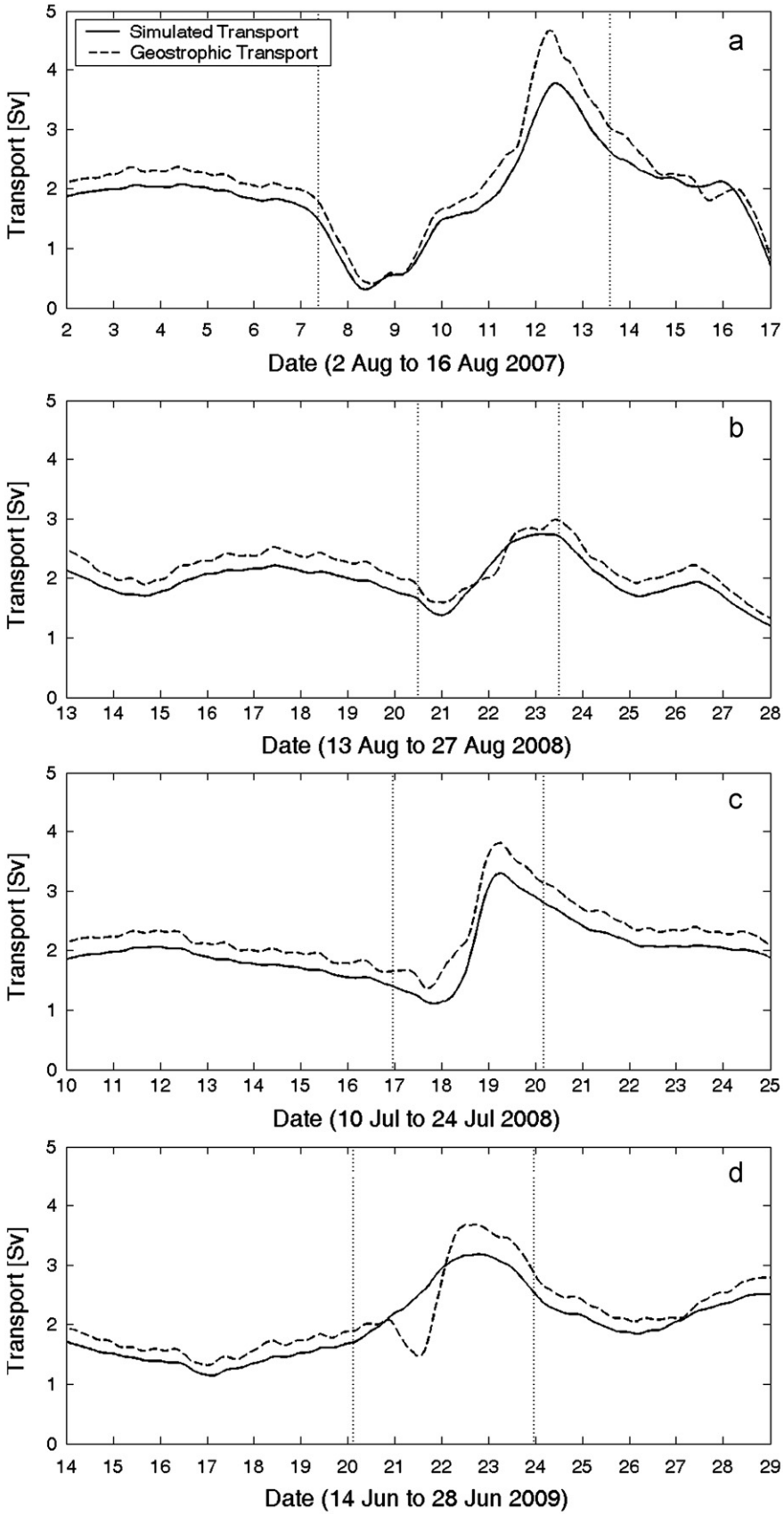

Fig. 9. Comparisons between the simulated transport and the geostrophic transport calculated from cross-strait sea surface slopes according to geostrophic balance during Typhoons (a) Pabuk (2007), (b) Nuri (2008), (c) Kalmaegi (2008), and (d) Linfa (2009). The time period between two vertical dotted lines in every panel is the period of influence of the typhoon on the Taiwan Strait.

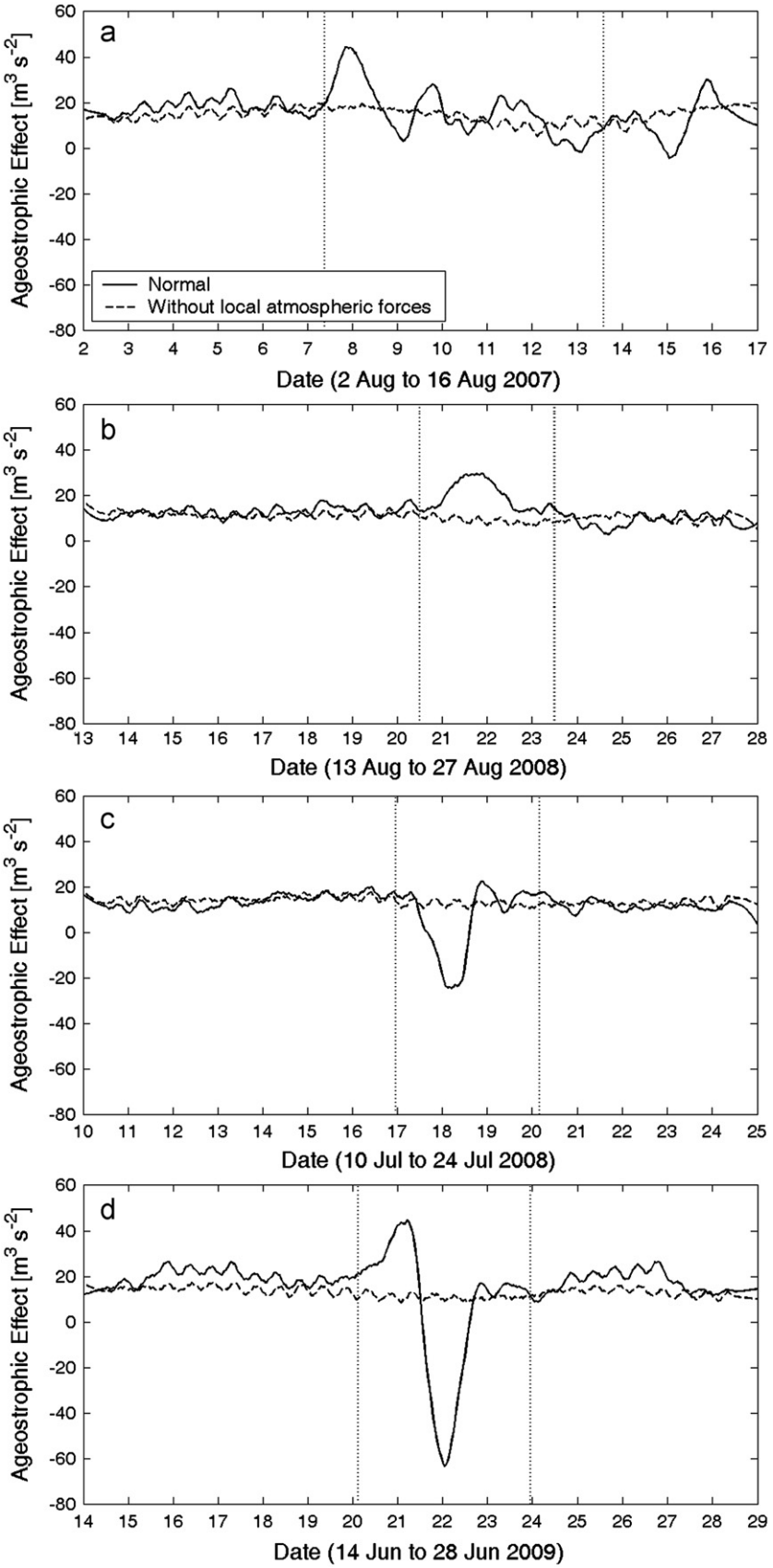

Fig. 10. Comparisons of ageostrophic effects between simulated with full forces (normal) and simulated without local atmospheric forces (treatment) during Typhoons (a) Pabuk (2007), (b) Nuri (2008), (c) Kalmaegi (2008), and (d) Linfa (2009). The time period between two vertical dotted lines in every panel is the period of influence of the typhoon on the Taiwan Strait.

conducted a numerical experiment in which local atmospheric forces inside the Taiwan Strait were masked and other configurations of the model were kept unchanged. The results for the ageostrophic effect from the experiment are shown in Fig. 10 and those simulated with full forces (normal results) are also provided for comparison. The results without local atmospheric forces were quite close to the mean values of the normal results throughout the four periods considered, indicating that the remote forcing effect determined the background or fundamental component of the ageostrophic effect. However, small fluctuations in the experimental results demonstrated that the remote forcing effect had little contribution to the variation of the ageostrophic effect: being less than 43% standard deviation before the typhoons obviously influenced the strait and less than 26% during the periods of influence. Therefore, the violent change of the ageostrophic effect was associated with local atmospheric forces rather than remote forcing effects during these typhoon events.

The following conclusion was drawn: the change of transport was mainly determined by atmospheric forcing, the ageostrophic effect and bottom friction acting together. Whether a typhoon enhanced northward transport through the Taiwan Strait depended to a great extent on its track relative to the strait. The typhoon was favorable if it travelled westward in the area south of the strait or moved northward along the west bank of the strait. A prophase weak southward and anaphase strong northward along-strait wind stress was necessary and crucial in enhancing northward transport. The ageostrophic process, mainly generated by local atmospheric forces, was relatively complicated. It first stored some energy from atmospheric forcing to restrain the change of transport, and then it released the stored energy to prolong and even to intensify the enhanced northward transport.

Acknowledgments

This work was jointly supported by the National Natural Science Foundation of China (41076002 and 41276007), the Fundamental Research Funds for the Central Universities (2010121036), the Science Foundation of Fujian Province (2010Y0064) and the Public Science and Technology Research Funds Projects of Ocean (200905013-7). The buoy data were provided by the Fujian Province Ocean and Fishery Bureau. The blended wind data were obtained from the CERSAT, at IFREMER, Plouzané, France (http://cersat.ifremer.fr/layout/set/print/data/) and the mean sea level air pressure data were downloaded from the ECMWF Data Server (http://data-portal.ecmwf.int/). The current data were taken from the Climate Prediction Center of the National Weather Service (http://www.cpc.ncep.noaa.gov/products/GODAS/), USA. Professor John Hodgkiss of The University of Hong Kong is thanked for polishing the English.

References

Chai, F., Xue, H., Shi, M., 2001. The study of horizontal transport in the Taiwan Strait. Oceanography in China 13, 168–177. (in Chinese with English abstract).
China Meteorological Administration, 2006. Grade of Tropical Cyclones (GB/T 19201—2006). The General Administration of Quality Supervision, Inspection and Quarantine and the Standardization Administration of the People's Republic of China, Beijing, China, 10 pp (in Chinese).
Chang, Y.-C., Tseng, R.-S., Centurioni, L.R., 2010. Typhoon-induced strong surface flows in the Taiwan Strait and Pacific. Journal of Oceanography 66, 175–182.
Chen, C.T.A., Liu, C.T., Chuang, W.S., Yang, Y.J., Shiah, F.K., Tang, T.Y., Chung, S.W., 2003. Enhanced buoyancy and hence upwelling of subsurface Kuroshio waters after a typhoon in the southern East China Sea. Journal of Marine Systems 42, 65–79.
Chuang, W.S., 1985. Dynamics of subtidal flow in the Taiwan Strait. Journal of the Oceanographical Society of Japan 41, 65–72.
Fang, G., Wei, Z., Choi, B.H., Wang, K., Fang, Y., Li, W., 2003. Interbasin freshwater, heat and salt transport through the boundaries of the East and South China Seas from a variable-grid global ocean circulation model. Science in China, Series D: Earth Sciences 46, 149–161.
Flather, R.A., 1976. A tidal model of the north-west European continental shelf. Mémoires Société Royale des Sciences de Liège 6 (10), 141–164.
Fu, Z., Hu, J., Yu, G., 1991. Seawater flux through Taiwan Strait. Chinese Journal of Oceanology and Limnology 9, 232–239.
Guo, J.S., Hu, X.M., Yuan, Y.L., 2005. A diagnostic analysis of variations in volume transport through the Taiwan Strait using satellite altimeter data. Advances in Marine Science 23, 20–26. (in Chinese with English abstract).
Jan, S., Sheu, D.D., Kuo, H.M., 2006. Water mass and throughflow transport variability in the Taiwan Strait. Journal of Geophysical Research 111, C12012.
Ko, D.S., Preller, R.H., Jacobs, G.A., Tang, T.Y., Lin, S.F., 2003. Transport reversals at Taiwan Strait during October and November 1999. Journal of Geophysical Research 108 (C11), 3370.
Lin, S.F., Tang, T.Y., Jan, S., Chen, C.J., 2005. Taiwan strait current in winter. Continental Shelf Research 25, 1023–1042.
Lin, Y.H., Fang, M.C., Hwung, H.H., 2010. Transport reversal due to Typhoon Krosa in the Taiwan Strait. The Open Ocean Engineering Journal 3, 143–157.
Marmorino, G.O., 1983. Small-scale variations of the wind-driven coastal sea-level response in the West Florida Bight. Journal of Physical Oceanography 13, 93–102.
Pedlosky, J., 1987. Geophysical Fluid Dynamics. Springer-Verlag New York Incorporation, New York.
Pettigrew, N. R., 1981. The dynamics and kinematics of the coastal boundary layer off Long Island. Ph.D. thesis, Massachusetts Institute of Technology, 262 pp.
Tsai, Y., Chern, C.S., Wang, J., 2008. Typhoon induced upper ocean cooling off northeastern Taiwan. Geophysical Research Letters 35, L14605.
Wang, Y.H., Jan, S., Wang, D.P., 2003. Transports and tidal current estimates in the Taiwan Strait from shipboard ADCP observations (1999–2001). Estuarine, Coastal and Shelf Science 57, 193–199.
Wu, C.-R., Hsin, Y.-C., 2005. Volume transport through the Taiwan Strait: a numerical study. Terrestrial Atmospheric Oceanography Science 16, 377–391.
Wyrtki, K., 1961. Physical oceanography of the southeast Asian waters. NAGA Report Volume 2, unpublished.
Zhang, W.-Z., Hong, H.-S., Shang, S.-P., Chen, D.-W., Chai, F., 2007. A two-way nested coupled tide-surge model for the Taiwan Strait. Continental Shelf Research 27, 1548–1567.
Zhang, W.-Z., Hong, H.-S., Shang, S.-P., Yan, X.-H., Chai, F., 2009. Strong southward transport events due to typhoons in the Taiwan Strait. Journal of Geophysical Research 114, C11013.